Earth, Planets and Space

FULL PAPER

Open Access

Blind study site assessment of shear-wave velocity at Kumamoto City, Japan, using direct-fitting SPAC methods

Michael Asten[1*], Aysegul Askan[2] and Shaghayegh Karimzadeh[3]

Abstract

The study used data acquired by the ESG6 Blind Prediction Step BP1 Working Group for purposes of facilitating a comparison of interpretation methods for obtaining shear-wave velocity profiles (V_s) from array observations of microtremor (passive seismic) noise. This work uses the direct-fitting MMSPAC method and the krSPAC method on passive seismic data supplied from four seven-station nested triangular arrays with apertures ranging from 1 to 962 m, located within Kumamoto City, Japan. The data allow a useful frequency range of 38 Hz down to 0.3 Hz, giving depth sensitivities from 2 m to > 1000 m. Results are presented as a seven-layer model which has time-averaged shear wave velocities for top 30 m and 300 m of $V_{s30} = 189$ m/s and $V_{s300} = 584$ m/s, respectively. HVSR spectra show two significant peaks at 1.2 and 0.35 Hz which are indicative of major V_s contrasts at depths 26 m and 750 m. The MMSPAC method (and its krSPAC variant) also proved viable on one asymmetric array where four of the seven stations were corrupted by incoherent low-frequency noise. Indications of a lateral variation in V_s could be detected due to the non-concentric geometry of the four arrays, and also from variations in HVSR spectra at stations of the largest array. Further analysis in step 4 of the blind trials, making use of geological data and a Preferred model supplied to participants, showed apparent discrepancies between the Preferred and our BP1 model for the upper 40 m where a supplied PS log appears to be inconsistent with geological data and the blind BP1 model. At low frequencies 0.5–2.5 Hz dispersion data and the BP1 model suggest that use of the Rayleigh effective mode is superior to use of the fundamental mode in deducing the Vs model at depths below 100 m. The method of direct fitting of model and observed SPAC spectra used in MMSPAC also enabled the use of a bandwidth 0.5–38 Hz for interpretation, which is a wider bandwidth than that achieved by other participants for use of passive seismic data alone.

Keywords Site effect, Microtremor, Passive seismic, SPAC, MMSPAC, krSPAC, Blind prediction

*Correspondence:
Michael Asten
michael.asten.monash@gmail.com
Full list of author information is available at the end of the article

Graphical Abstract

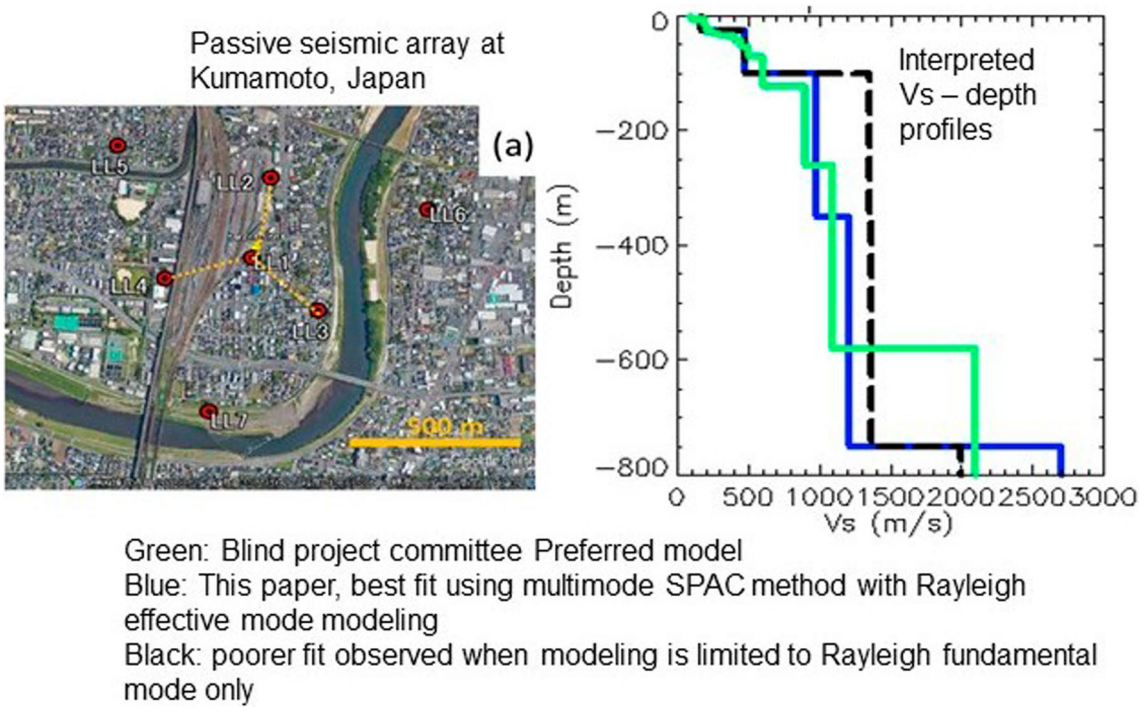

Introduction

In this paper, we first describe a blind interpretation of passive seismic data. An additional section then describes how the interpretation compares with a reference model supplied by Committee organizing the blind trial after all participants submitted blind interpretations.

The study used data acquired by the ESG6 Blind Prediction Step 1 (BP1) Working Group for purposes of facilitating a comparison of interpretation methods for obtaining shear-wave velocity profiles from array observations of microtremor (passive seismic) noise. Data from Kumamoto city (Fig. 1a) were supplied for nested triangular 7-station arrays with apertures ranging from 1 to 962 m. This interpretation utilized the method of direct fitting of multimode spatially averaged coherency (MMSPAC) with iterative layered-earth (1D) modelling to minimize least-square error between observed and model SPAC spectra.

Data were supplied for five arrays labelled LL, M, SM, S and SS1, having apertures (maximum triangle side lengths) of 962, 243, 78, 20 and 2 m. Figures 1a and 2a show locations of arrays LL and M, respectively. The small arrays SM, S and SS1 were located close to station M4 shown in Fig. 2a. Exact locations of each array and instrument specifications are given in Blind Project Committee (2019).

(See figure on next page.)

Fig. 1 **a** Array geometry showing seven receivers in two nested triangles. There are six station separation distances r1–r6 available for spatial averaging of coherency spectra. For array S, large side-length r4 = 20 m, and the six interstation distances r1–r6 are 5.8, 10.0, 11.5, 20.0, 10.0 and 17.6 m. **b** Locality of arrays for microtremor observations in Kumamoto City, Japan. Centre of the array is at 32.775641°N, 130.687920°E. Red circles show a pair of nested triangles side lengths 481 and 962 m. **c** SPAC spectra for a small array near the center of (**b**) using a triangle side-length 10 m. Black line—observed SPAC; red and blue lines—model SPAC spectra for the fundamental Rayleigh mode R_0 and the effective mode R_e. The fitting is performed by least squares using the R_e curve. Thick black horizontal line—the frequency range used in the curve fitting. **d** and **e** HVSR spectra and SPAC spectra for the radial separations (yellow dotted lines each of length 277 m) of stations LL2, LL3, LL4 from center LL1 in (**b**). Black line—observed spectra; red and blue lines—model spectra for the fundamental Rayleigh mode R_0 and the effective mode R_e; yellow, green lines—model spectra for modes R_2, R_3. **f**, **g** V_s profile interpreted by fitting observed and model SPAC spectra for all six array triangles including the two shown in this figure. Strong velocity contrasts in V_s at depths 26 m and 750 m are the primary cause of the HVSR peaks at 1.2 Hz and 0.35 Hz

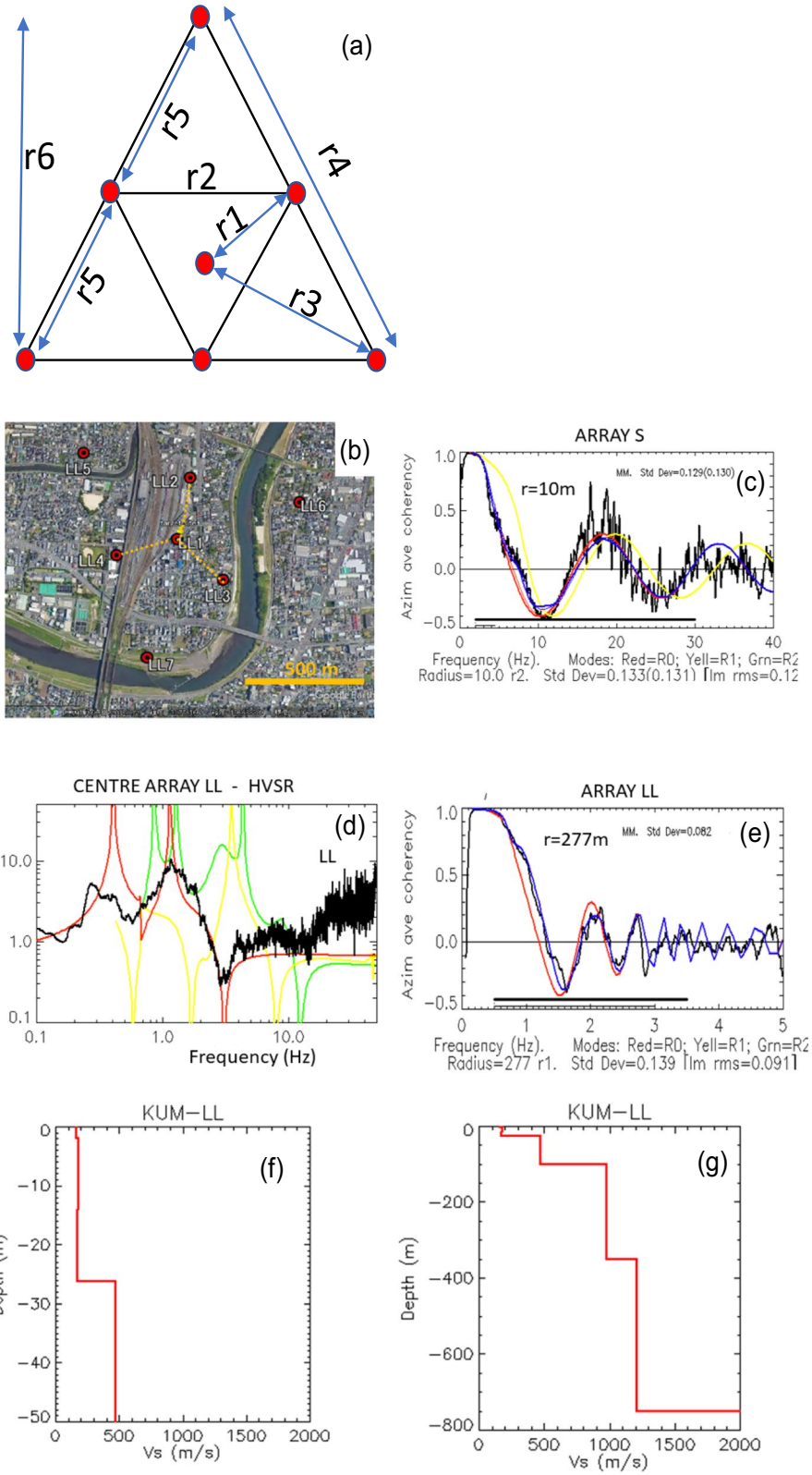

Fig. 1 (See legend on previous page.)

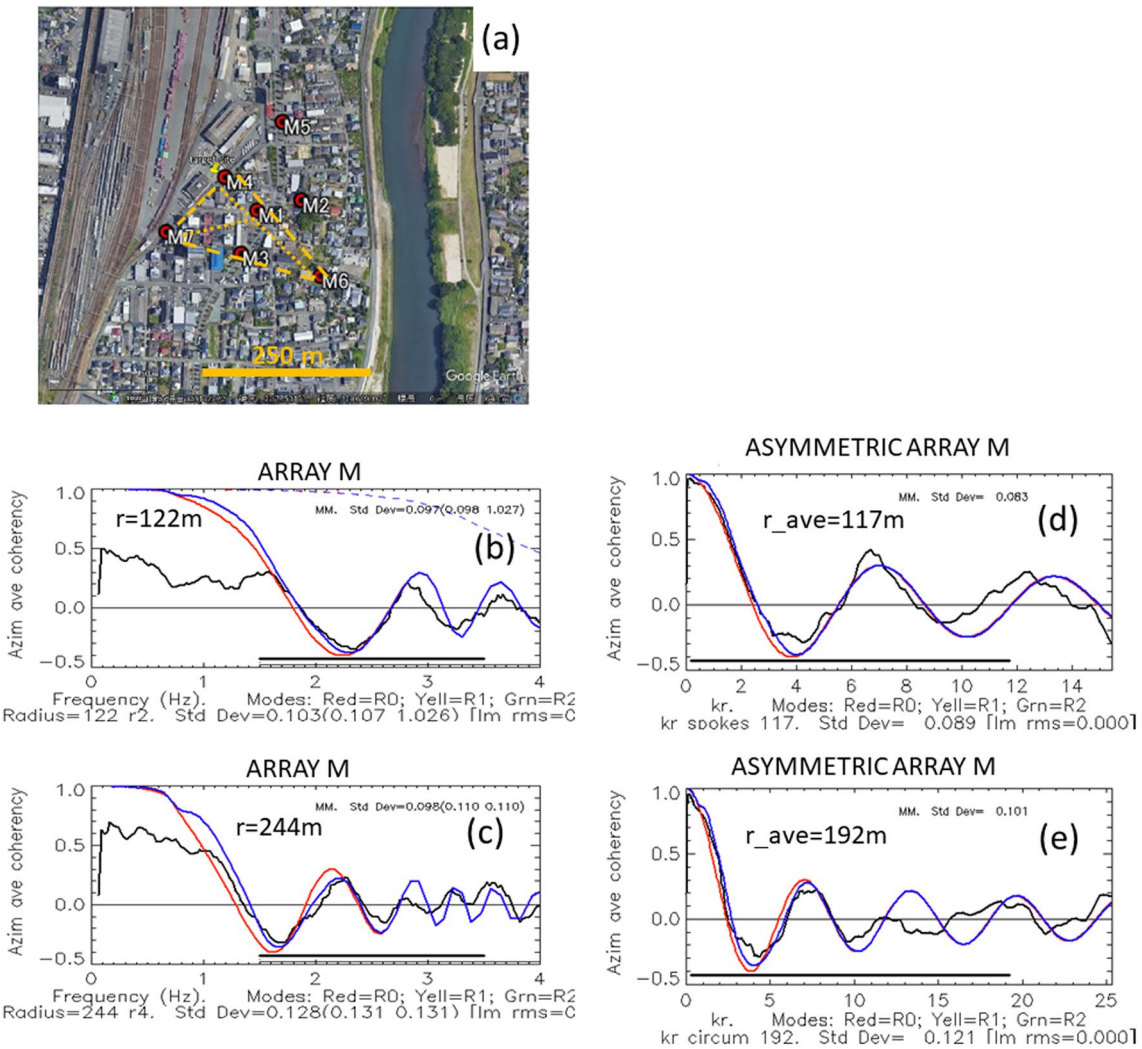

Fig. 2 **a** Locality for mid-size arrays in Kumamoto City, Japan. Dotted yellow lines—the "radii" of an asymmetric "triangle" centered on M1. Dashed yellow—sides of the asymmetric triangle. Red circles show a pair of nested triangles side lengths 122 and 244 m. Stations M2, M3, M5 are corrupted by low-frequency noise below1.5 Hz. Small arrays SM, S and SS1 (apertures 78, 20 and 2 m) are centered close to station M4. **b**, **c** SPAC spectra for the inner, outer triangles of array M, apertures 122, 244 m. Colors as for Fig. 1. Thick black line—the frequency range 1.5–3.5 Hz used in the curve fitting. **d**, **e** krSPAC spectra for the (unequal) radii and (unequal) sides (average lengths 117 and 192 m respectively) of the asymmetric traingle shown in (**a**). Thick black line—the *kr* range used in the curve fitting, equivalent to an extended frequency range 0.5–3.5 Hz

Purpose of microtremor studies in assessing earthquake hazard

The soil characteristics of any site significantly affect the amplitude, frequency content and duration of the earthquake ground motion records measured at the ground surface of that location (e.g., Stone et al. 1987; Seed et al. 1990; Ameri et al. 2009; Bradley 2012; Massa et al. 2014; Barani and Spallarossa 2017). It is thus important to consider local site properties in both probabilistic and deterministic hazard analyses. For a standard classification of sites and use in ground motion models, hazard analyses as well as building codes, time-averaged shear-wave velocity (V_s) to a depth of 30 m (V_{S30}) has been a globally accepted metric (e.g., Dobry et al. 2000; Yong 2016). However, to accurately assess the physical effects related to local site conditions in surface ground motions, it is important to carefully estimate the structure deeper than the top 30 m, preferably down to the bedrock layer. Particularly for deterministic hazard assessments which require analyses beyond empirical ground motion models, information on a deeper structure via 1D, 2D or even 3D velocity models at sites or regions of interest becomes crucial (e.g., Magistrale et al. 2000; Asten et al. 2014; Askan et al. 2015). The backbone of multi-dimensional

models is 1D profiles well resolved both spatially and depthwise. Thus, in this study we obtain 1D velocity models with the joint use of MMSPAC and HVSR methods in order to report V_{S30}, V_{S100} and V_{S300}.

Processing of Kumamoto City microtremor data

Coherency estimates

Time series were selected to minimize the inclusion of obvious spikes and the selected time series were transformed to spectra by fast Fourier transform (FFT), then complex coherencies for all interstation pairs of vertical-component records were computed by averaging in the frequency domain in windows with a width of 40 frequencies, where the frequencies are set by the FFT. The process is described by Asten (2006).

The smoothed interstation coherencies were then azimuthally averaged. Each 7-station array permits coherencies to be azimuthally averaged over six different station spacings. Figure 1a illustrates these station spacings for array S.

The interpretation method used facilitates the identification of multiple modes of Rayleigh-wave propagation and hence the method is named multimode spatially averaged coherency (MMSPAC). The azimuthally averaged coherencies are termed MMSPAC and hence there are 6 MMSPAC plots produced for each seven-station array having the geometry shown in Fig. 1a.

Interpretation by the MMSPAC direct fitting algorithm

The methodology is described extensively by Asten and Hayashi (2018) and Hayashi et al. (2022). Those papers also describe the differences between MMSPAC which performs direct fitting of SPAC spectra, and conventional SPAC interpretation which fits observed and model dispersion curves. Layered-earth model dispersion curves were computed using the forward modelling routines sdisp (Herrmann 2013). In all interpretation here, the forward models computed the 1st four Rayleigh modes which are then combined to provide the effective mode R_e (which assumes that Rayleigh wave energy is generated by vertical-impact sources at the earth surface). The algorithm for R_e is described by Ikeda et al. (2012). Using the computed R_e mode model dispersion, the model SPAC curves were computed; these are then fitted to the observed MMSPAC plots. Parameters of the layered earth (thickness h and shear-wave velocity V_s) are then iteratively varied until a best fit (standard deviation) between the observed and model SPAC is obtained over a specified bandwidth.

The use of the R_e mode in SPAC interpretation is not always necessary for accurate results, but where layer boundaries exist with strong velocity contrasts, the R_e mode generally improves results. For the layered-earth model derived for this site, we find that there is a deviation between the fundamental R_o mode and the effective R_e mode for frequency bands 1–2 Hz, 7–14 Hz and 20–40 Hz. Thus, there is reason to believe that the R_e mode will yield greater accuracy in layered-earth V_s estimates. This point is discussed further in section "Further analysis of results in step BP4".

Starting model

A starting model was generated using parameters from the Chimoto model (Layers 1 to 6) and the J-SHIS deep data set (layers 7–11), provided by the Blind Project Committee (2019). Depth of the water table was not provided but in view of the fact that the survey area is surrounded by rivers, a notional water table depth of 2 m is used in this study. Layers below 2 m are therefore assumed saturated and ascribed a V_p of 1500 m/s (see discussion on V_p/V_s ratios in Asten and Hayashi 2018).

Problem with Array SS1

The miniature array SS1 yields frequencies up to 40 Hz on the MMSPAC curves but the layered earth model produced includes an apparent near-surface compact layer 1 ($V_{s1} = 479$ m/s). However, this layer is not consistent with the MMSPAC curves of array S and hence the array SS1 was discarded. The result with SS1 is a puzzle because it is obvious from photos that both SS1 and S were located on a sealed parking lot and existence of a compacted top layer is believable. However, the array S data are quite clear in not permitting such a layer.

Useful frequencies

The direct-fitting MMSPAC algorithm generally allows the use of a wider bandwidth in interpretation than that of the methods based on dispersion-curve fitting.

At this site, we achieved direct fitting of observed and modelled SPAC spectra over frequency ranges as follows:

Array S: 2 to 30 Hz.
Array SM: 1 to 20 Hz.
Array M: 1 to 2.5 Hz.
Array LL: 0.5 to 3.5 Hz.

The range of useful frequencies achieved with the passive data and the MMSPAC direct-fitting algorithm (maximum 30 Hz) indicates that the use of active surface wave methods is not required at this site.

HVSR

The MMSPAC method uses only vertical-component seismic noise at each station in inversion for a layered-earth model. Horizontal:vertical spectral ratios (HVSR) are also used to show spectral peaks in the data and compare with modelled ellipticity of fundamental and higher modes of Rayleigh waves. These comparisons assist in

validation of the inverted model since strong peaks are associated with S-wave resonances at layer interfaces showing a strong velocity contrast.

Layered earth interpretation from MMSPAC on all arrays

Figure 1 shows the location of the large array LL; smaller arrays lie within this footprint (Blind Project Committee 2019). Figure 1c and e also shows representative MMSPAC plots for the small S and the LL arrays. These plots illustrate the direct fitting of observed and model SPAC curves, where the observed data (black line) are fitted to the SPAC curve computed for the Rayleigh effective mode (blue) generated by the final layered-earth model. The plots also include for reference the modelled SPAC for the fundamental (red) and first higher (yellow) Rayleigh modes, but these are not used in the fitting process. Further details appear in Asten and Hayashi (2018), (Fig. 4). The plots clearly show the range of usable frequencies used in the interpretations, from a high of 30 Hz for the S array, to a low of 0.5 Hz for the LL array. Plots of the HVSR in Fig. 1d show two dominant peaks at 1.2 Hz and 0.35 Hz indicating resonances associated with two major shear-wave velocity contrasts associated with the depth to the base of layer 5 and of layer 8 (depths 26 m and 750 m).

Figure 1f and g shows the final best-fit V_s profiles interpreted for the set of arrays at the Kumamoto site, in the blind trial BP1. Time-averaged V_s for the top 30 m and 300 m are $V_{s30}=189$ m/s and $V_{s300}=584$ m/s, respectively. Table 1 shows the best-fit model obtained by the MMSPAC process for all arrays in the BP1 step 1 blind trial. This is the 1D model used by the authors for the subsequent steps BP2 and BP3 modeling of earthquake strong motion at the site (Askan et al. 2022).

Table 1 Best-fit layered-earth model for the Kumamoto site, BP1 Step 1

H	VP	VS	RHO
2	279	161	1.80
4	1500	181	1.90
8	1500	181	2
2.3	1500	170	2
10	1500	170	2.1
75	1500	470	2.1
251.1	2600	980	2.2
400	2600	1210	2.2
498	5000	2700	2.50
1041	5500	3200	2.65
1000	6000	3400	2.75

H, VP, VS, Rho denote layer thickness (m), P and S-wave velocities (m/s), and density (t/m^3)

Problem with array M

Figure 2a shows the position of array M. It has issues due to three very noisy seismometer records (Nos. M2, M3, M5). It is likely that these seismometers were affected by local noise from machinery or buried pipes or cables. Exclusion of these seismometers leaves a highly asymmetric triangular array; however, SPAC processing was still possible using the krSPAC method of processing; this method performs spatial averaging of coherency spectra by transforming the frequency axis of spectra to a dimensionless form given by kr, where k is the wavenumber and r is the spatial separation of an individual pair of seismometers (Asten et al. 2019).

Figure 2b, c shows results of modelling the two triangles using conventional MMSPAC and it is obvious that noise has made SPAC data at frequencies below 1.5 Hz useless. However, the results of MMSPAC fitting of observed and model SPAC spectra in kr space on the asymmetric triangle of noise-free stations, shown in Fig. 2d, e, demonstrate that useful curve fitting is possible for a low frequency limit of 0.5 Hz.

Lateral variation across array LL

SPAC methods are generally limited to one-dimensional interpretation of variations in V_s with depth. However, different positions of array centers and variations in HVSR spectra provide two insights into possible lateral variations in the V_s structure.

The first indicator is a variation in V_s within the upper 300 m. Array M lies within the eastern half of Array LL. There is a resolvable difference in layer 7 from the two arrays ($V_{s7}=810$ m/s for Array M; $V_{s7}=980$ m/s for Array LL, both at depth range 100–350 m). This observation suggests softer ground at depth 100 + m in the eastern half of Array LL.

The second indicator uses the HVSR spectra for the outer stations of array LL, plotted in Fig. 3. HVSR for these stations show similar shaped ~ 0.35 Hz peaks (associated with depth 750 m on Fig. 1f) for stations LL6 (north-east), LL7 (south) and stations from smaller arrays. However, station LL5 (north-west) has a different shape although similar in frequency. Figure 3 shows the HVSR spectra for the total horizontal component, and for separate components Nr/V and Er/V, where Nr and Er are orthogonal horizontal components for a chosen rotation angle from north. A rotation angle of 20–30 degrees maximizes the separation of Nr/V and Er/V, and this may be indicative of a strike direction at the associated depths of order 750 m. The reduced size of the composite HVSR peak at LL5 may indicate a lateral change to lower V_s in the basement rocks to the north-west, in the vicinity of the 750 m depth.

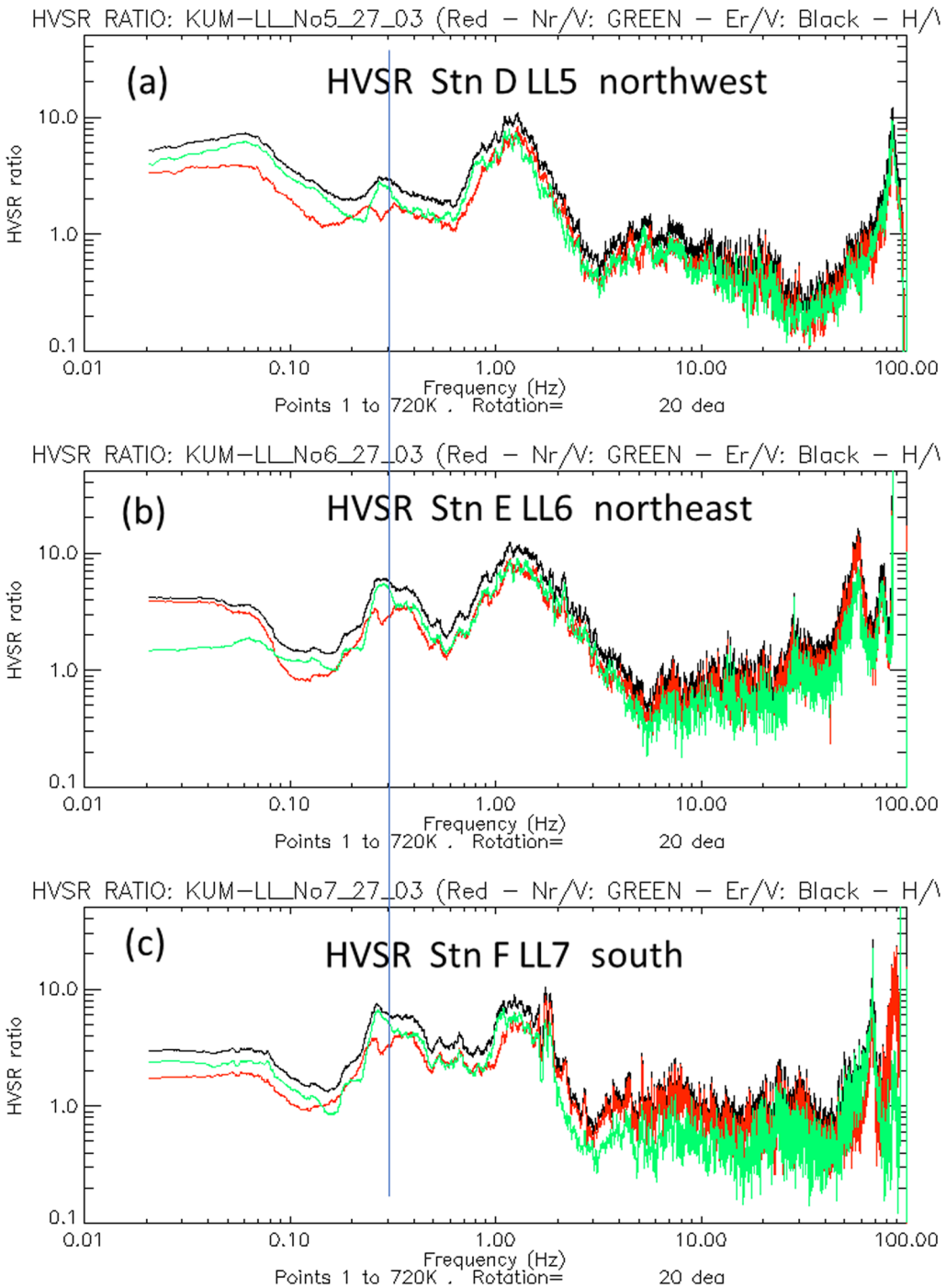

Fig. 3 HVSR spectra for array LL vertices, showing (black) H/V, (red) Nr/V and (green) Er/V, where Nr and Er are orthogonal components of N and E horizontal signal rotated by 20 degrees from north. The vertical blue line shows that the 0.3 Hz HVSR peak for station LL5 is clearly anomalous

Conclusions from blind study BP1

Array analysis of microtremor noise at Kumamoto using the direct fitting MMSPAC method provides a high-quality shear-wave velocity V_s profile. Four of the five arrays give consistent profiles, with the small array SS1(1 m aperture) being anomalous, possibly due to variations in surface compaction. The useful frequencies range from a high of 30 Hz to a low of 0.5 Hz, resolving V_s over a depth range from 2 m to > 1000 m.

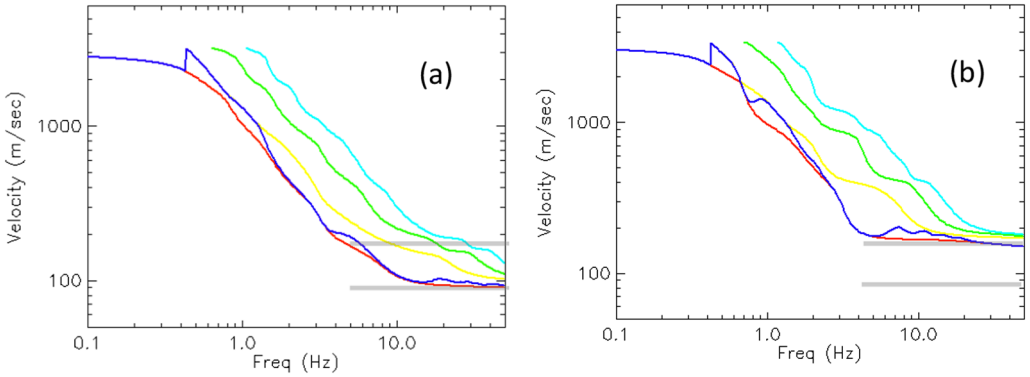

Fig. 4 **a** Model dispersion curves for Rayleigh mode computed for the blind project committee's Preferred layered-earth model. Red, yellow, green, blue are modes R_0, R_1, R_2, R_3. Blue is the effective mode R_e. **b** Model dispersion curves computed for the best-fit model described in this paper, as listed in Table 1. Horizontal grey lines indicate the discrepancy between the two sets of dispersion curves for frequencies 5–40 Hz

It appears that the use of active seismic surface wave methods is not necessary at this site.

HVSR spectra show two significant peaks at 1.2 and 0.35 Hz which are indicative of major V_s contrasts at depths 26 m and 750 m.

One array M (aperture 210 m) was not useable as a symmetric array due to presence of incoherent noise at frequencies below 1.5 Hz on three of the seven stations. However, the use of the krSPAC algorithm allowed the analysis of the remaining asymmetric array of four stations, yielding a consistent V_s profile.

Indications of a lateral variation in V_s were detected at depth range of 100–350 m (lower V_s under the eastern part of the survey area). An anomalous HVSR peak for the north-west vertex of array LL suggests a possible change in basement character or V_s at depths of order 750 m.

The layered earth model developed in this study BP1 was subsequently used to provide a V_{s30} value and an input velocity model for use in step BP2 and step BP3, respectively, of the blind trial project (Askan et al. 2022). These studies demonstrated the application of the BP1 model to both probabilistic and deterministic earthquake hazard assessments.

Further analysis of results in step BP4 with inclusion of preferred (Reference) model

Analysis of discrepancies between preferred and authors' BP1 models

Following submission of blind interpretations by all participants (step BP1), a Preferred layered-earth model and geological data were released by the Committee for purposes of reanalysis and discussion (step BP4). Figure 4 shows the model dispersion curves for five modes of Rayleigh-wave propagation for both the Preferred model and the authors' step BP1 model. Two strong discrepancies are obvious: (a) the R_0 mode for 10–40 Hz on the Preferred model is close to half the values shown for the authors' BP1 model, and (b) For frequencies ranging from 0.4 to 1.5 Hz, the BP1 model has larger differences between the phase velocities for the R_0 and R_e modes than does the Preferred model.

The differences between the two models are also evident in Fig. 5 which shows the examples of observed SPAC spectra together with spectra modelled using the R_e dispersion curve for the Preferred and the BP1 models. Figure 5a uses an example of data from the S array, station separation 10 m, and shows a standard deviation of 0.14 for the best fit of observed and BP1 model spectra at frequencies 2–38 Hz. The equivalent standard deviation for the preferred model is 0.24. Figure 5b shows similarly using the LL array, station separation 277 m; for the frequency band of 0.5–2.5 Hz, the corresponding standard deviations are 0.06 (BP1) and 1.7 (Preferred).

Figure 6a shows V_s logs for the upper 40 m of the Preferred and our BP1 models. Geological data are provided from a borehole of depth 39 m, located close to station LL5 (see Fig. 1a, and also Oyo 2020). The borehole has also been logged with P and S-wave velocities but the velocity values and ratio between P and S-wave values appear anomalous; those downhole P and S-wave values appear to have been incorporated in the preferred model and may therefore partially explain discrepancy (a) above. We believe that the geological and SPT logs in Fig. 6c together with the observed SPAC data in Fig. 5 give support to our BP1 model.

Detection of a near-surface low velocity layer

The geological log in Fig. 6b shows a layer of sand-silt at depth 20–29 m. This zone also shows as a relatively soft layer in the standard penetration test (SPT) log in Fig. 6b, underlain by harder gravels (from Oyo 2020). Comparing

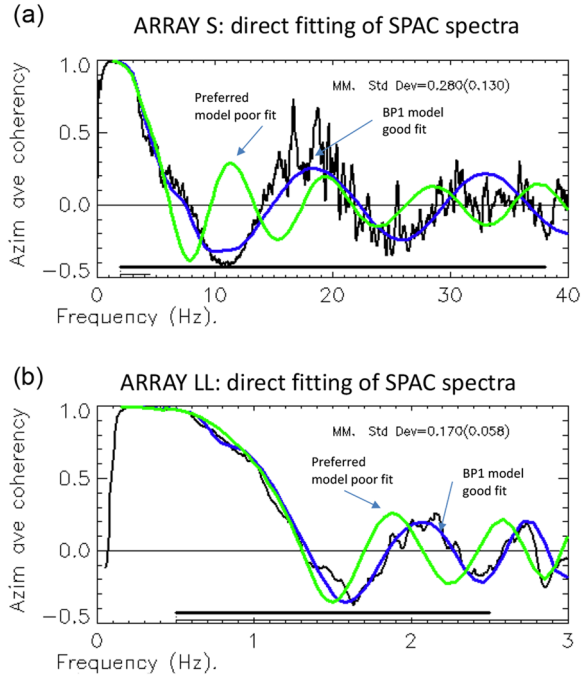

Fig. 5 **a** SPAC spectra for Preferred model compared with BP1 model, for station separation 10 m. Black: observed SPAC; Green: Preferred model effective mode; Blue: BP1 model effective mode. Standard deviation of fit computed over frequencies 2–38 Hz shows: Std dev for Preferred model is poor; 0.28, Std dev for BP1 model is fair; 0.13 **b** SPAC spectra for Preferred model compared with BP1 model, for station separation 277 m. Colors as for (**a**) Standard deviation of fit computed over frequencies 0.5–2.5 Hz shows: Std dev for Preferred model is poor; 0.17, Std dev for BP1 model is good; 0.06

this geological and SPT data with our BP1 interpreted V_s profile, we see an affirmative correlation of an interpreted low-velocity layer (LVL), estimated to be 14–25 m depth, and underlain by a significant V_s contrast estimated at 25 m depth. These values, however, are about 20% shallower than boundaries shown in the geological and SPT logs.

The results relating to the prediction and subsequent affirmation of existence of the LVL when using the method of MMSPAC are consistent with the discussion of the LVL challenge provided in Asten and Hayashi (2018). The Preferred model does not show the existence of the LVL.

Detection of a major V_s velocity contrast at 580 + m

Figure 6c compares the interpreted models for V_s to a depth of 800 m for the Preferred model and the authors' BP1 model. Both models show a major increase in V_s at depth (580 m and 750 m respectively). This velocity contrast is significant in that it is the principal cause of the 0.4 Hz peak in HVSR data, noted in Fig. 1d.

Achievable bandwidth for interpretation

The direct fitting of observed and model SPAC spectrum enabled the use of passive seismic data over the frequency range of 0.5–30 Hz. Of the remaining 27 submissions of BP1 interpretations, one also showed a maximum usable frequency with passive data of 30 Hz, and four showed a maximum of 20 Hz. Eight submissions used active-source data to achieve an equivalent or higher maximum frequency for data inversion to a V_s profile.

The result achieved here using the direct-fitting MMSPAC method which is similar to that found in comparisons provided by an earlier blind trial (Asten et al. 2022) which found that the use of the direct-fitting MMSPAC method allowed interpretation to a higher frequency limit than most other passive seismic methods with the exception of seismic noise interferometry.

Reduction of bias in V_s profiles via use of Rayleigh wave effective mode

There is some indication that the use of Rayleigh effective-mode modelling reduces bias in estimates of the V_s profile. Figure 6c shows the authors' best-fit V_s model to depth 800 m when limiting phase velocity models to the Rayleigh fundamental mode only. The V_s profile is obviously biased to higher velocities in this case; quantitatively we compute $V_{s300} = 584$ m/s and 655 m/s, respectively, for the effective mode and the fundamental mode interpretations.

The results of the blind trial step BP1 for all participants are summarized graphically by Blind Project Committee (2021). There are 28 submissions, and simple inspection shows that four submissions can be excluded due to very large deviations from the preferred model; 19 of the remaining 24 submissions show the submitted V_s profile clearly biased towards higher V_s values compared with the preferred model over the depth interval 100-500 m. The remaining five submissions (including the authors' BP1 model) show

(See figure on next page.)

Fig. 6 **a** Green: Vs depth profile for the Preferred model. Blue: Vs depth profile for the authors' BP1 model. **b** Geological log and SPT log (Oyo 2020) supplied to blind project participants after submission of individual analyses of surface-wave data. Diagonal blue lines indicate top and bottom of a soft low velocity later shown independently by this blind interpretation and by the borehole SPT log. **c** Green and blue: The Preferred model and the authors' best-fit BP1 Vs profiles are plotted for depths 0–800 m. Black dashed: an alternative interpretation made in this paper using Rayleigh-wave fundamental-mode analysis only

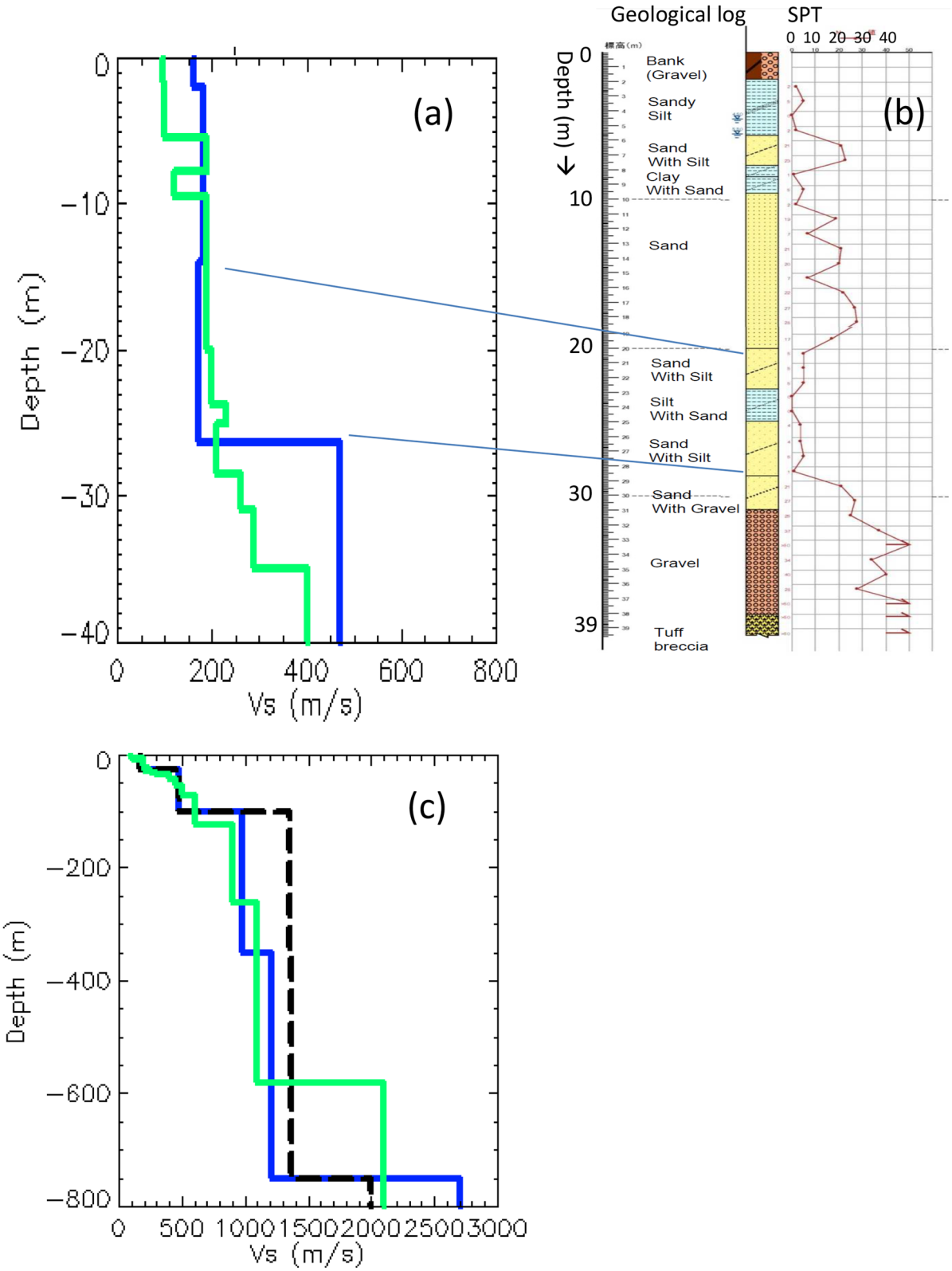

Fig. 6 (See legend on previous page.)

some overlap with the preferred model over this depth interval.

Depths of 100–500 m correspond approximately to frequencies in the range of 0.8–2 Hz when using the Rayleigh wave depth sensitivity guideline of a half-wavelength, and as shown in Fig. 4b it is this frequency band which shows that the effective mode shifted to phase velocities higher than the fundamental mode. This argument is qualitative in nature, but it allows us to propose the hypothesis that the inversion of phase velocity dispersion data using fundamental-mode modelling only may be a cause of bias of interpreted V_s profiles to higher velocities than those present in the real earth. The hypothesis may be tested quantitatively when tabular data for all submitted V_s profiles together with details of modelling algorithms used become available.

Abbreviations

ESG	Effects of surface geology
Vs	Shear-wave velocity
SPAC	Spatially averaged coherency or spatial autocorrelation
MMSPAC	Multimode SPAC
krSPAC	Wavenumber normalized SPAC
HVSR	Horizontal to vertical spectral ratio
SPT	Standard penetration test
LVL	Low velocity layer

Acknowledgements
The blind trial was organized by the ESG6 Local organizing committee (Blind Project Committee, 2019). Submission to special issue on ", Earth Planets and Space.

Author contributions
MA analysed microtremor array data to the level of V_s profiles. AA and SK assessed applicability to earthquake hazard models, and used the results for subsequent submissions to step 2 and step 3 of the blind trials. All authors read and approved the final manuscript.

Funding
Not applicable.

Availability of data and materials
Data are available from the reference given (Blind Project Committee 2019).

Declarations

Ethics approval and consent to participate
Not applicable.

Consent for publication
The Blind Project Committee invited this publication.

Competing interests
The authors declare that they have no competing interests.

Author details
[1]Earth Insight, Hawthorn, Vic, Australia. [2]Civil Engineering and Earthquake Studies Departments, METU, Ankara, Turkey. [3]Civil Engineering Department, ISISE, University of Minho, Guimarães, Portugal.

Received: 28 September 2022 Accepted: 6 March 2023
Published online: 20 March 2023

References

Ameri G, Massa M, Bindi D, D'Alema E, Gorini A, Luzi L, Marzorati S, Pacor F, Paolucci R, Puglia R, Smerzini C (2009) The 6 April 2009 Mw 6.3 L'Aquila (Central Italy) earthquake: strong-motion observations. Seismol Res Lett 80:951–966

Askan A, Karimzadeh S, Asten M, Kilic N, Şişman FN, Erkmen C (2015) Assessment of seismic hazard in the Erzincan (Turkey) region: construction of local velocity models and evaluation of potential ground motions. Turkish J Earth Sci 24:529–565

Askan A, Karimzadeh S, Asten M (2022) Use of stochastic finite fault simulation method for a target Mw=5.5 event, 2016 Kumamoto foreshock (Mw=6.5) and mainshock (Mw=7.0) at blind test sites. Earth Planets Sp. https://doi.org/10.21203/rs.3.rs-2223236/v1

Asten MW (2006) On bias and noise in passive seismic data from finite circular array data processed using SPAC methods. Geophysics 71:V153–V162

Asten MW, Hayashi K (2018) Application of the spatial auto-correlation method for shear-wave velocity studies using ambient noise. Surv Geophys 39:633–655. https://doi.org/10.1007/s10712-018-9474-2

Asten M, Askan A, Ekincioglu EE, Sisman FN, Ugurhan B (2014) Site characterization in northwestern Turkey based on SPAC and HVSR analysis of microtremor noise. Explor Geophys 45:74–85. https://doi.org/10.1071/EG12026

Asten MW, Stephenson WJ, Hartzell S (2019) Spatially averaged coherencies (krSPAC) and Rayleigh effective-mode modeling of microtremor data from asymmetric arrays. Geophysics 84:EN47–EN56. https://doi.org/10.1190/geo2018-0524.1

Asten MW, Yong A, Foti S, Hayashi K, Martin AJ, Stephenson WJ, Cassidy JF, Coleman J, Nigbor R, Castellaro S, Chimoto K, Cornou C, Cho I, Hayashida T, Hobiger M, Kuo C-H, Macau E, Mercerat D, Molnar S, Pananont P, Pilz M, Poovarodom N, Sáez E, Wathelet M, Yamanaka H, Yokoi T, Zhao D (2022) An assessment of uncertainties attributed by analysts, array types and processing algorithms for microtremor observations, using the phased 2018 COSMOS Blind Trials. J Seismolog 26:757–780. https://doi.org/10.1007/s10950-021-10059-4

Barani S, Spallarossa D (2017) Soil amplification in probabilistic ground motion hazard analysis. Bull Earthq Eng 15:2525–2545

Blind Project Committee (2019) http://sds.dpri.kyoto-u.ac.jp/esg6-bp/DocumentBPstep1.pdf. Accessed 27 Sept 2022

Blind Project Committee (2021) BP4-Specifications after the results of BP1(20210504).pdf. https://drive.google.com/file/d/1aSbF7qqgvYIze7YFM0SgRhCQY_wY8YEl/view?usp=sharing. Accessed 27 Sept 2022

Bradley BA (2012) Strong ground motion characteristics observed in the 4 September 2010 Darfield, New Zealand earthquake. Soil Dyn Earthq Eng 42:32–46

Dobry R, Borcherdt RD, Crouse CB, Idriss IM, Joyner WB, Martin GR, Power MS, Rinne EE, Seed RB (2000) New site coefficients and site classification system used in recent building seismic code provisions. Earthq Spectra 16:41–67

Hayashi K, Asten M, Stephenson W, Cornou C, Hobiger M, Pilz M, Yamanaka H (2022) Microtremor array method using SPAC analysis of Rayleigh-wave data. J Seismolog 26:601–627. https://doi.org/10.1007/s10950-021-10051-y

Herrmann RB (2013) Computer programs in seismology: an evolving tool for instruction and research. Seismol Res Lett 84:1081–1088. https://doi.org/10.1785/0220110096

Ikeda T, Matsuoka T, Tsuji T, Hayashi K (2012) Multimode inversion with amplitude response of surface waves in the spatial autocorrelation method. Geophys J Int 190:541–552. https://doi.org/10.1111/j.1365-246X.2012.05496.x

Magistrale H, Day S, Clayton RW, Graves R (2000) The SCEC southern California reference three-dimensional seismic velocity model version 2. Bull Seismol Soc Am 90:S65–S76

Massa M, Barani S, Lovati S (2014) Overview of topographic effects based on experimental observations: meaning, causes and possible interpretations. Geophys J Int 197:1537–1550

Oyo (2020) Kumamoto Eq. Ground Structure Survey. https://sds.dpri.kyoto-u.ac.jp/esg6-bp/Kumamoto%20Eq.%20Ground%20Structure%20Survey.pdf. Accessed 27 Sept 2022

Seed RB, Dickenson SE, Reimer MF, Bray JD, Sitar N, Mitchell JK, Idriss IM, Kayen RE, Kropp A, Harder LF, Power MS (1990) Preliminary report on the principal geotechnical aspects of the October 17, 1989 Loma Prieta

earthquake. Report UCB/EERC-90/05, Earthquake Engineering Research Center, University of California, Berkeley.
Stone WC, Yokel FY, Celebi M, Hanks T, Leyendecker EV (1987) Engineering aspects of the September 19, 1985 Mexico earthquake. NBS Building Science Series 165. National Bureau of Standards, Washington
Yong A (2016) Comparison of measured and proxy-based Vs30 values in California. Earthq Spectra 32:171–192

Publisher's Note